Author/s:
Vacante, F;Rodor, J;Lalwani, MK;Mahmoud, AD;Bennett, M;De Pace, AL;Miller, E;Van Kuijk, K;De Bruijn, J;Gijbels, M;Williams, TC;Clark, MB;Scanlon, JP;Doran, AC;Montgomery, R;Newby, DE;Giacca, M;O'Carroll, D;Hadoke, PWF;Denby, L;Sluimer, JC;Baker, AH

Title:
CARMN Loss Regulates Smooth Muscle Cells and Accelerates Atherosclerosis in Mice

Date:
2021-04-30

Citation:
Vacante, F., Rodor, J., Lalwani, M. K., Mahmoud, A. D., Bennett, M., De Pace, A. L., Miller, E., Van Kuijk, K., De Bruijn, J., Gijbels, M., Williams, T. C., Clark, M. B., Scanlon, J. P., Doran, A. C., Montgomery, R., Newby, D. E., Giacca, M., O'Carroll, D., Hadoke, P. W. F. ,... Baker, A. H. (2021). CARMN Loss Regulates Smooth Muscle Cells and Accelerates Atherosclerosis in Mice. Circulation Research, 128 (9), pp.1258-1275. https://doi.org/10.1161/CIRCRESAHA.120.318688.

Persistent Link:
https://hdl.handle.net/11343/265895

CARMN Loss Regulates Smooth Muscle Cells and Accelerates Atherosclerosis in Mice

Francesca Vacante[1], Julie Rodor[1], Mukesh K. Lalwani[1], Amira D. Mahmoud[1], Matthew Bennett[1], Azzura De Pace[2], Eileen Miller[1], Kim Van Kuijk[3], Jenny deBruijn[3], Marion Gijbels[4,5], Thomas C. Williams[6], Michael B. Clark[7], Jessica P. Scanlon[1], Amanda C. Doran[8], Rusty Montgomery[9], David E. Newby[1], Mauro Giacca[10], Dónal O'Carroll[2], Patrick W.F. Hadoke[1], Laura Denby[1]*., Judith C. Sluimer[1,3]*, Andrew H. Baker[1,3 #]

[1]Queens Medical Research Institute, BHF Centre for Cardiovascular Sciences, University of Edinburgh; [2]Institute for Regeneration and Repair, Centre for Regenerative Medicine, University of Edinburgh; [3]Pathology, Maastricht Medical Center, the Netherlands; [4]Medical Biochemistry, Experimental Vascular Biology, Amsterdam UMC, University of Amsterdam; [5]Pathology CARIM, Cardiovascular Research Institute Maastricht, GROW-School for Oncology and Developmental Biology, Maastricht University; [6]Insitute of Genetics and Molecular Medicine, University of Edinburgh; [7]Centre for Stem Cell Systems, Department of Anatomy and Neuroscience, The University of Melbourne; [8]Medicine, Vanderbilt University Medical Center, Nashville, US; [9]miRagen Therapeutics, lnc. Boulder, Colorado, and; [10]King's College London.

* Authors contributed equally to the work.

Running title: CARMN Regulates Atherosclerosis via SMC Modulation

Circulation Research

Subject Terms:
Animal Models of Human Disease
Coronary Circulation
Mechanisms
Smooth Muscle Proliferation and Differentiation
Vascular Biology

Address correspondence to:
Dr. Andrew H. Baker
University of Edinburgh
Queen's Medical Research Institute
47 Little France Crescent
Edinburgh, UK, EH16 4TJ
Tel: +44 131 24 26728
Andy.Baker@ed.ac.uk.

ABSTRACT

Rationale: In the microenvironment of atherosclerotic lesions, vascular smooth muscle cells (vSMCs) switch to a dedifferentiated state but the underlying molecular mechanisms driving this switch are not fully understood. Long noncoding RNAs (lncRNAs) are dysregulated during vascular pathology, but relatively little is known about their involvement in controlling vSMCs function. *CARMN* is a lncRNA located immediately upstream of the microRNAs (miRNAs) miR-143 and miR-145, both involved in vSMCs function.

Objective: We investigated the role of the lncRNA *CARMN*, independent from miR-143 and miR-145, as potential a regulator of vSMC phenotypes *in vitro* and the consequences of its loss during the development of atherosclerosis *in vivo*. We hypothesized that loss of CARMN is a primary event controlling the functional switch towards pro-atherogenic vSMC phenotype and accelerates the development of the plaques *in vivo*.

***Method and Results*:** Expression of *CARMN* lncRNA was silenced using GapmeRs in human coronary arterial smooth muscle cells (hCASMCs), revealing that GapmeR-mediated loss of CARMN negatively affects miR-143 and miR-145 miRNA expression. RNA sequencing of CARMN-depleted hCASMCs revealed large transcriptomic changes, associated with vSMC proliferation, migration, inflammation, lipid metabolism and dedifferentiation. The use of miR-143 and miR-145 mimics revealed that CARMN regulates hCASMC proliferation in a miRNA-independent manner. In human and mouse, CARMN and associated miRNAs were downregulated in advanced versus early atherosclerotic lesions. Using a CRISPR-Cas9 knock-out approach, we explored the implications of CARMN depletion during atherosclerosis in vivo. Consistent with *in vitro* results, the knock-out of CARMN impaired the expression of miR-143 and miR-145 under homeostatic conditions. Importantly, when atherosclerosis was induced in these mice, CARMN knock-out increased the volume, size, pro-inflammatory LGALS3-expressing cells content and altered plaque composition, yielding an advanced phenotype.

Conclusions: We identified the early loss of CARMN lncRNA as critical event which primes vSMCs towards a pro-atherogenic phenotype *in vitro* and accelerates the development of atherosclerosis in vivo.

Keywords:
Cholesterol, non-coding RNA, smooth muscle cells, vascular biology, atherosclerosis.

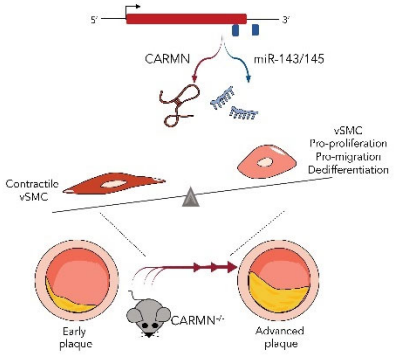

Nonstandard abbreviations and Acronyms:

AAV: adeno-associated virus
ABCA1: ATP-binding Cassette Transporter 1
ABCG1: ATP-binding Cassette Subfamily G Member 1
Acta2: Smooth muscle actin 2
ApoE: apolipoprotein E
ASO: antisense oligonucleotides
αSMA: α-Smooth Muscle Actin
CARMN: cardiac mesoderm enhancer-associated noncoding RNA
$CARMN^{-/-}$: CARMN knock-out
$CARMN^{+/+}$: CARMN wild type
CCL: Chemokine C-C Motif Ligand
CD68: Cluster of Differentiation 68
CD45: Protein Tyrosine Phosphatase Receptor Type C
CMBCD: cholesterol-methyl-β-cyclodextrin
CXCL1: C-X-C Motif Chemokine 1
CNN1: Calponin 1
COL3a1: Collagen type 3 alpha chain 1
CRISPR: Clustered Regularly Interspaced Short Palindromic Repeats
EdU: 5-ethynyl-2'-deoxyuridine
EGFR: Epidermal Growth Factor Receptor
FACS: fluorescence-activated cell sorting
FISH: Fluorescent In-Situ Hybridization
hCASMCs: human coronary artery smooth muscle cells
KLF4: Kruppell-like factor 4
IL1-beta: Interleukin 1 beta
IL6: Interleukin 6
ISH: In-Situ Hybridization
LCM: laser capture microdissection
$LDLR^{-/-}$: low density lipoprotein receptor knock-out
Lgals3: Galectin 3
lncRNA: Long Noncoding RNA
Myh11: Myosin Heavy Chain 11
Myocd: Myocardin
MiRNAs: miRNAs
MMP: Metalloproteases
OPT: Optical Projection Tomography
ORO: Oil Red O
Ox-LDL: Oxidised Low-Density Lipoprotein
PCSK9: Proprotein Convertase Subtilisin/Kexin type 9
PDGF: Platelet-Derived Growth Factor
PDFGRa: Platelet-Derived Growth Factor Receptor alpha
qRT-PCR: Quantitative Real-Time Polymerase Chain Reaction
RNA-seq: RNA sequencing
RNU48: Small Nucleolar RNA 48
TAGLN: Taglin
TSS: Transcriptional Start Sites
UBC: Ubiquitin C
vSMCs: vascular smooth muscle cells

INTRODUCTION

Atherosclerosis is a chronic and inflammatory condition of the arterial branches and a leading cause of cardiovascular disease and cerebrovascular disease[1]. Vascular smooth muscle cells (vSMCs) have a critical and complex role in atherogenesis. In homeostatic conditions, adult vSMCs are largely quiescent and characterized by a specific gene expression pattern and functional properties which define their signature[2]. However, in response to pathological environmental stress signals that occur during atherogenesis, vSMCs lose their contractile signature and switch into a pro-atherogenic phenotype as they start to proliferate, migrate and lose their typical markers (such as Smooth Muscle Actin Alpha 2) [3–5]. In particular, during the formation of stable plaques, vSMC proliferation and migration toward the intimal layer are associated with the formation of a stabilizing fibrotic cap[6]. Whereas, during the latter stages of disease, the recruitment and activation of inflammatory cells, the decrease in collagen content and increase in metalloprotease secretion contribute to the breakdown and dynamic remodeling of the fibrotic cap and the progression towards rupture-prone plaques[7]. Therefore, it is critical to unravel and fully understand these complex regulatory networks to be able to target specific molecular mechanisms during the progression of atherosclerosis.

Recently, several studies have demonstrated that non-coding RNAs, namely long non-coding RNAs (lncRNAs) and miRNAs (miRNAs), are crucial regulators of many pathophysiological processes during atherosclerosis [8–10]. Namely, miRNAs miR-143 and miR-145 have been found to be important regulators of vSMC differentiation and disease-associated phenotypic switching in response to pro-atherogenic stimuli such as cholesterol loading (water-soluble cholesterol)[11] or PDGF-BB treatment[12–16]. Their functions have also been highlighted in several mouse models, where the ablation of both miR-143 and miR-145 induced spontaneous neointimal lesions in the femoral artery[14 17], dysregulated signaling pathways[14], and regulated vSMC migration [17]. However, despite numerous studies uncovering the importance of miR-143 and miR-145 in diverse disease conditions [14–16,18–22], their function and regulation remains conflicting in the context of atherosclerosis [16,19].

A long noncoding RNA (lncRNA), named CARMN, is juxta-positioned upstream from miR-143 and miR-145[23]. This lncRNA was originally identified in human cardiomyocytes and named Cardiac Mesoderm Enhancer-associated Noncoding RNA (CARMN) [24 25]. Previous studies have demonstrated that a crosstalk may exist between the processing of lncRNA host genes, such as CARMN, and encoded miRNAs [26] and that the biogenesis of these noncoding molecules might be mutually exclusive[27] and produced RNAs with independent functions[28]. Although the functions of miR143 and miR145 have been explored, whether CARMN has an independent function is not completely elucidated in the context of atherosclerosis. Here, we demonstrated that CARMN has a function independent from miR-143 and miR145 in regulating vSMC proliferation, while vSMC migration or dedifferentiation processes are regulated through the modulation of miRNA expression in hCASMCs. Moreover, we uncovered a pivotal role of the CARMN/miRNA locus during the pathophysiology of atherosclerotic disease in vivo and demonstrated that in CARMN knockout mice, the development of atheroma was accelerated when compared to wild type mice, thereby inducing advanced and more vulnerable plaques.

METHODS

Data Availability.

Expanded information about materials and methods are available in the Online Data Supplement. All supporting data and materials are available within the Online Data Supplement and available from the corresponding author upon reasonable request. All RNA-Seq data are deposited in the Gene Expression Omnibus database (Ref. GSE158972 and Ref. GSE165445).

RESULTS

Expression and subcellular localisation of CARMN lncRNA and associated miRNAs in primary human CASMCs under basal and stimulated conditions.

We first sought to understand the expression and regulation of *CARMN* in hCASMCs together with miRNAs miR-143 and miR-145. Publicly available data in Ensembl database 98 show several transcript variants belonging to the complex *CARMN* locus (Figure 1 A). Initially, we assessed the expression levels of individual isoforms in hCASMCs, using isoform-specific primers when possible (only isoform 4 was amplified in combination with isoform 9) (Figure 1 A). Expression data indicated that all the isoforms were detectable in hCASMCs (Figure 1 B). Following this, we used common primers capturing all isoforms except 205 and 211, to assess the expression levels of *CARMN* (Figure 1 A). Based on previous studies, the function of lncRNAs is related to their subcellular localization[29,30], therefore, we next determined the localization of *CARMN* in hCASMCs. Subcellular fractionation as well as RNA-FISH indicated that *CARMN* predominantly localized in the nuclear compartment of hCASMCs (Online Figure I A, B). Of note, during the course of these experiments, there was a new release of the Ensembl annotation that includes 7 new potential isoforms (Online Figure II A), yet all remained detectable by our common primer set. However, considering that lncRNA annotation is not definitively accurate and that lncRNA are expressed in a cell-specific way, we applied a transcript discovery pipeline to publicly available RNA-Seq data of hCASMCs obtained by ENCODE (https://www.encodeproject.org/), which did not reveal the existence of un-annotated additional isoforms (Online Figure II A). This analysis also showed that the 3' end of the most abundant *CARMN* transcripts is upstream of the miR143/miR145 loci (Online Figure II A). Moreover, we carried out 5' Rapid Amplification of cDNA Ends and long-reads sequencing (Oxford Nanopore technology). Both techniques revealed the presence of main transcriptional start site (TSS), already described in the annotation, but also detected minor additional (TSS) (Online Figure II B, C). Moreover, the long-read sequencing revealed 4 major exonic structures all covered by the current annotation and not including miR143/145 (Online Figure II D). In addition, we found reads mapping to the miR-143/145 stem-loop which suggested the existence of fragments from the processed pri-miRNA with different 5' end, one of them shared by *CARMN* transcripts (Online Figure II E). Altogether, these analyses confirmed the complexity of *CARMN* locus.

Platelet-derived growth factor (PDGF-BB) is one of the main pathogenic cytokines released at the site of injury with a potent mitogen action to vSMCs [31]. To gain insight into the regulation of *CARMN* in proliferating VSMCs, we treated serum-starved hCASMCs with PDGF-BB for 48 hours (Figure 1 C) and assessed the levels of *CARMN*. *CARMN* was significantly downregulated following PDGF-BB stimulation (Figure 1 D). Levels of expression of miR-143 and miR145 were also significantly decreased (Figure 1 D). It is well established that vSMC migration from the media to the intima is critically involved in the pathophysiology of vascular disease, although a difficult process to quantify in human lesions[4]. We therefore assessed whether *CARMN* was dynamically regulated under migratory stimuli. A scratch was made in a monolayer of serum-starved hCASMCs, and the levels of *CARMN* and miR-143/145 were assessed at 5, 10 and 24 hours after scratching (Figure 1 E). However, no statistical difference was observed in the lncRNA or microRNAs expression in scratched versus control cells (Figure 1 F). Additionally, we characterized the expression of the lncRNA *CARMN* in primary culture of hCASMCs following the treatment with water-soluble cholesterol-methyl-β-cyclodextrin (CMBCD), for 72 hours (Figure 1 G). CMBCD loading substantially decreased the expression levels of *CARMN* versus control cells, and similarly the expression of miR-143 and miR-145 (Figure 1 H) as previously described [11]. Moreover, we observed similar pattern of decrease in *CARMN* expression using another model of hCASMC dedifferentiation towards foamy cell-like phenotype [32] by loading cells with oxidised Low-Density Lipoproteins (ox-LDL) (Online Figure III A-C). Thus, the expression levels of *CARMN* lncRNA and associated miRNAs are

reduced by the exposure to proliferative stimuli and CMBCD loading of hCASMCs, which is a critical process during the pathophysiology of atherosclerosis.

Knockdown of the human CARMN axis drives the phenotypic transition of hCASMCs towards a pro-atherogenic phenotype.

To assess the functional importance of *CARMN*, we utilised an LNA-GapmeR antisense oligonucleotide (ASOs) approach. We designed two different GapmeRs targeting the introns of *CARMN* isoforms (named GapCARMN and GapCARMN2) (Figure 1 A). Following transfection of hCASMCs with GapCARMN and GapCARMN2, we observed a significant knockdown of *CARMN* versus a GapmeR Control (GapCTR) using the common primers (Figure 2 A, Online Figure III D). Importantly, we confirmed the downregulation of *CARMN* at the isoform level using isoform-specific primers (Online Figure III E). Notably, the levels of miR-143 and miR-145 were also significantly downregulated following GapCARMN and GapCARMN2 transfection in CASMCs (Figure 2 A and Online Figure III D). Furthermore, to support the results obtained with intronic-targeting GapmeR (GapCARMN/GapCARMN2), we used a previously described GapmeR targeting the exonic region of *CARMN* transcripts (named GapCARMN3 in this manuscript)[25] and confirmed similar changes (Online Figure IV A).

To understand the role of *CARMN* in hCASMCs in physiological and pathological conditions, we analyzed the transcriptomic changes associated with the *CARMN*-axis depletion using GapCARMN in untreated hCASMCs (basal), as well as following stimulation upon proliferation, migration or CMBCD loading (Figure 2 B). The expression of *CARMN* was firstly assessed in RNA-seq samples to validate appropriate knockdown (Online Figure IV B). Following RNA sequencing analysis, principal component analysis (PCA) confirmed clustering of the sample replicates and showed a clear separation of the GapCARMN-treated samples from the GapCTR-treated hCASMCs in all analyzed conditions (Online Figure IV C). The PCA also confirmed an effect of the different treatments at the transcriptomic level. In particular, we noted the clear separation of the CMBCD-treated cells from their relevant control cells (Basal_C), showing the strong effect of this stimulus on the hCASMC transcriptome. We also noticed the proliferation-stimulated samples showed an intermediate phenotype which can be explained by different responses due to the diverse cell culture densities of the hCASMCs as well as the point of harvesting following GapmeR transfection. We analyzed the significant changes in gene expression in GapCARMN versus GapCTR treated cells for each condition (Online Figure IV D) and found that *CARMN* depletion affected a large number of genes, on average 910 genes per condition with 411 up-regulated and 499 down-regulated genes. In total, we found 2315 genes whose expression was significantly changed by *CARMN* depletion and analyzed their expression profiles (Figure 2 C). The heatmap revealed a largely consistent effect of CARMN-axis depletion, independent of hCASMC treatment. Gene ontology analysis of the CARMN-axis dependent genes in basal conditions already revealed the enrichment of several processes related to vSMC phenotypic transition towards de-differentiated phenotype (Figure 2 D). More specifically, we noted enrichment of terms linked to a positive effect on cell migration and proliferation that are key processes during atherogenesis. Moreover, we investigated whether the depletion of CARMN-axis affects the transcription factor regulating vSMC homeostasis, Myocardin (Myocd)[33]. However, Myocd was undetectable in both our RNA-Seq and by qRT-PCR analysis (Online Figure IV E, F). Interestingly, *CARMN*-dependent genes were also involved in lipid metabolism and cholesterol homeostasis. *CARMN* depletion also upregulated the expression of pro-inflammatory cytokine genes such as interleukins (IL1-beta, IL6) associated with atherosclerosis progression and CXCL1 and as well as CCL2 chemokines responsible of leucocyte migration and recruitment to the developing lesions (Figure 2 E) [34,35]. Furthermore, we noted a significant upregulation of matrix metalloproteinase 1 (MMP1) and a significant downregulation of collagen and elastase genes (COL3a1 and ELN), with expression decreasing in the context of extracellular matrix remodelling and plaque vulnerability (Figure 2 E) [36,37]. Genes regulated by *CARMN* and involved in positive regulation of proliferation, migration, regulation of inflammatory response and response to lipid are reported in Online Data set II. Related to the enrichment of 'lipid' terms in the gene

ontology analysis, the heatmap of *CARMN* regulated genes revealed the clustering of CMBCD treated samples transfected with GapCTR among all GapCARMN samples, further suggesting that *CARMN*-dependent genes were also affected by CMBCD treatment (Figure 2 C). Therefore, we directly compared the genes regulated by *CARMN* in basal condition with genes changed upon CMBCD treatment. Importantly, we found that about 50% of CMBCD-regulated genes were altered in the same direction upon *CARMN* depletion (Figure 2 F), suggesting that *CARMN* depletion alone promotes a water-soluble cholesterol loaded-like phenotype in the absence of CMBCD co-incubation. These results show the impact of *CARMN* depletion on hCASMCs transcriptome and in particular on cholesterol-regulated genes. Collectively, these results suggest *CARMN* knock-down might be an important event which primes vSMCs to the phenotypical transition occurring in plaques formation and progression.

Knockdown of CARMN-axis lncRNA activates proliferation, migration and induces partial dedifferentiation of hCASMCs in vitro.

Considering the results obtained from the transcriptomic analysis of *CARMN* silenced hCASMCs, we further deciphered the functional consequence of *CARMN* axis silencing on hCASMC phenotypes. Interestingly, the depletion of *CARMN* significantly increased the proliferation of hCASMCs in quiescent conditions (0.2%FBS) or under PDGF-BB stimulation (Figure 3 A, B). Next, we assessed the effect of *CARMN* depletion on hCASMC migration. Although the response to the migratory stimulus did not show significant difference in the expression levels of endogenous *CARMN* and miR-143/145, the downregulation of *CARMN* increased the migration rate of hCASMCs versus cells transfected with GapCTR (Figure 3 C, D). To further validate the involvement of *CARMN* in hCASMC CMBCD-induced dedifferentiation process, we analysed mRNA expression changes of the smooth muscle identity markers, Actin Alpha 2 (*Acta2*) and Myosin Heavy Chain11 (*Myh11*), and activated macrophage-like genes, Cluster of Differentiation 68 (*CD68*) and Galectin 3 (*Lgals3*). We confirmed that *CARMN* depletion leads to significant decrease of *Acta2* and *Myh11* levels, with concomitant significant increase of *CD68* expression in basal conditions (Figure 3 E, F, G). However, we did not observe significant change in Lgals3 expression in *CARMN*-depleted hCASMCs when compared to control group (Figure 3 H). Moreover, we assessed the expression levels of Kruppell-like factor 4 (*KLF4*) in *CARMN*-depleted hCASMCs, previously associated with vSMC dedifferentiation phenotype[38]. We did not observe significant change in the expression of this transcription factor in *CARMN*-depleted proliferative or de-differentiating hCASMCs (Online Figure V A, B), indicating likely *KLF4*-independent effects. Instead, we observed a significant increase in *KLF4* in scratched hCASMCs with *CARMN*-depletion (Online Figure C). In order to robustly characterize hCASMCs phenotypic state following *CARMN* depletion, we also took into consideration other typical vSMCs marker genes such as Calponin1 (*CNN1*) and Taglin (*TAGLN*)[39,40]. However, their expression levels were not significantly changed following *CARMN* axis knockdown (Online Figure V D, E), therefore indicating that *CARMN* downregulation partially affects the vSMCs signature under unstimulated conditions. In addition, we investigated the expression of lipid-metabolism associated genes, such as *ABCA1* and *ABCG1*[11], which were found significantly upregulated following *CARMN* knockdown versus control (Online Figure V F, G). We did not observe the same pattern in the case of *Srebpf2*, *SCD* and *HMGS1* expression (Online Figure V H, I, J), indicating the modulation of *CARMN* partially primes the dedifferentiation towards a pro-inflammatory phenotype foam-cell like phenotype. These phenotypical changes observed in hCASMCs were confirmed with a second GapmeR, GapCARMN2 (Online Figure VI A-E). Collectively, these data suggest that the manipulation of the *CARMN* locus modulates the ability of hCASMCs to proliferate and migrate. In addition to this, the results obtained indicate that *CARMN* depletion affects the expression of some of the vSMC identity genes (*Acta2* and *Myh11*) and increases the levels of some of the CMBCD-regulated genes (*CD68*, *ABCA1*, *ABCG1*) priming vSMC to a partial dedifferentiation process.

CARMN depletion regulates hCASMCs proliferation in a miRNAs-independent manner.

As the GapmeR strategy to downregulate *CARMN* also affects the expression of the miRNAs, we designed a rescue experiment to assess the contribution of both *CARMN* and the miRNAs to the described phenotypes. We have applied a co-transfection approach to overexpress the levels of miRNAs by treatment with miR-mimic (mimic-143 and mimic-145) in combination with GapmeR-mediated *CARMN* knockdown. We first assessed the efficiency of this strategy confirming a significant upregulation in the expression of both miRNAs by qRT-PCR (Figure 4 A). Moreover, to assess their functional effect, we checked the expression of two miRNAs targets, *EGFR* and *PDGFRa* [41,12]. These were significantly downregulated following treatment with mimic143 and mimic145 (mimic143/145) versus mimic control (mimicCTR) (Online Figure VI F, G). In addition, we observed a significant upregulation of *CARMN* following treatment with miR143/145 compared to mimic control. While this increase might suggest a feedback loop in the modulation of *CARMN* expression induced by the hosted miRNAs (Figure 4 B), this modulation did not restore *CARMN* expression to its basal levels. We then co-transfected hCASMCs in basal conditions with GapmeR targeting *CARMN* (GapCARMN) concomitantly with mimic control (mimicCTR) or a combination of mimic-143 and mimic-145. *CARMN* knock-down increased hCASMCs proliferation while the overexpression of miR-143 and miR-145 did not significantly change the observed increase in cell proliferation. Therefore, *CARMN* appears to have independent effect on the modulation of hCASMCs proliferation at basal conditions (Figure 4 C). In contrast, miR-143/145 overexpression restored the levels of vSMC identity genes modulated by *CARMN* depletion, Acta2, Myh11 (Figure 4 D, E, F, G). In addition, the overexpression of miR-143/145 restored hCASMCs migration at basal levels thus rescuing the effects observed following *CARMN* depletion (Figure 4 H, I). Taken together, these results suggest that *CARMN* can regulate hCASMCs proliferation independent of miR-143 and miR-145 but that migration and dedifferentiation may be driven through *CARMN*-mediated regulation of the miRNAs.

The expression of CARMN lncRNA and associated miRNAs are downregulated in mouse and human advanced plaques.

To determine the relevance of *CARMN* in human atherosclerosis, we assessed the expression of the lncRNA in atherosclerotic plaques isolated from symptomatic patients undergoing carotid endarterectomy. Previous RNA-seq analysis performed in stable and unstable regions of human plaques[8], were interrogated and revealed a significant decrease of *CARMN* levels in the unstable region versus the stable plaques (Figure 5 A). Moreover, in the same RNA-Seq data, we interrogated the expression levels of previously identified *CARMN*-regulated genes. In agreement with the observations in *CARMN* knock-down samples, we found a significant upregulation of metalloproteinase (*MMP1*), significant downregulation of elastase (*ELN*) and a significant increase of pro-inflammatory genes (*IL1-beta* and *CCL2*) (Figure 5B), in unstable versus stable plaques, confirming our findings from *in vitro* studies through to human atherosclerosis.

To validate these findings, we analysed *CARMN* expression levels by qRT-PCR in carotid artery stenosis plaques isolated from different patients and confirmed the downregulation of the lncRNA in advanced versus early atheroma. Additionally, we showed the downregulation of miR-143 and miR-145 in the same samples (Figure 5 C). In order to identify the cellular localization of *CARMN* within human plaques, In Situ Hybridization (ISH) was performed in advanced stable plaques isolated from human carotid arteries of symptomatic patients. *CARMN* co-localized with α-Smooth Muscle Actin (*α-SMA*), typical marker for vSMCs and with CD68, marker of macrophages and dedifferentiated vSMCs within the plaques (Figure 5 D). Moreover, some *CARMN* RNAs co-localises with the CD45 marker[42] confirming the expression in immune cells. However, regions of the *CD68*/*CARMN* positive area appear negative for *CD45* in parallel sections, suggesting the possibility of a non-immune origin for these cells (Figure 5D).

As *CARMN* and miR-143/145 are evolutionary conserved, we were able to take advantage of mouse models to evaluate the expression and characterize the function of the *CARMN* locus. The mouse locus

harbours two annotated isoforms of *CARMN*, and their expression was analysed using a common primer. To further examine the role of the *CARMN* in the pathophysiology of disease, we assessed the expression of the lncRNA and the miRNAs at different stages of murine atherosclerosis. For this purpose, we investigated the levels of the *CARMN* locus in two groups of Low-Density Lipoprotein Receptor Knock Out mice ($LDLR^{-/-}$): i) mice fed with a 0.25% cholesterol diet for 14 weeks to develop advanced plaques, and ii) mice fed on regular chow for 14 weeks to promote the formation of early fatty streak. We first confirmed the plaque stage though qualitative histologic analysis classifying them as fatty streak, the first visible irregular lesion consisting of atherogenic lipoproteins and macrophages occurring at the lesion site [43], or advanced atheroma characterized by a large lipid-rich core, infiltrated macrophages and thin collagen-poor fibrotic cap [44] (Figure 5 E). Oil Red O (ORO) staining was performed to confirm plaques stages (Online Figure VII A).

We then isolated RNA from atherosclerotic lesions from each aortic root using Laser Capture Microdissection (LCM) and assessed the expression levels of the lncRNA and miRNAs. The murine *CARMN* as well as miR-143 and miR-145 were found significantly downregulated in advanced lesions versus early plaques (Figure 5 F), confirming the expression pattern observed in human advanced plaques.

CARMN axis knockout accelerates atherosclerosis in mice.

Considering the decrease of *CARMN* in advanced human and murine plaques and *in vitro* vSMC functional data, we hypothesized that the loss of murine *CARMN* would modulate the development of atherosclerosis in vivo. Therefore, we exploited a CRISPR/Cas9-mediated gene editing approach to constitutively knock-out ($^{-/-}$) the *CARMN* locus. The first exon of the *CARMN* transcripts and a 4.8kb portion of the gene promoter were deleted, leaving exons 2/3 and the miRNA stem loops intact (Figure 6 A). Aortas of mice on normal diet were used to confirm the deletion at the RNA level by RT-qPCR using primers directed at exon 1 versus wild type controls ($CARMN^{+/+}$) (Figure 6 B). Using isoform specific primers downstream of the deletion site, we confirmed the knock-down of both transcripts (Online Figure VII B, C). We also observed in the same samples the downregulation of miR-143 and miR-145. Moreover, as part of the characterization of knockout mice we examined the expression of the lncRNA Braveheart, downstream to *CARMN* transcript, which was previously found to be downregulated following loss-of-function of *CARMN* in mouse culture of CPCs[8]. However, qRT-PCR data indicated that Braveheart expression was not significantly changed in aortic arches isolated from $CARMN^{-/-}$ versus $CARMN^{+/+}$ samples (Online Figure VII, D). To determine the effect of *CARMN* deficiency in the pathological context, we induced atherosclerosis in $CARMN^{-/-}$ mice and C57BL/6Ntac littermate controls using a validated mouse model of atherosclerosis [3] (Figure 6 C). To achieve long-term hypercholesterolemia, 8-weeks old $CARMN^{+/+}$ and $CARMN^{-/-}$ mice were injected with 10^{12} vector genomes/mouse of the recombinant Adeno-associated Virus serotype 8 (AAV8) to induce overexpression of Proprotein convertase subtilisin/Kexin type 9 (PCSK9) in the liver. From one-week post injection, all mice received high cholesterol diet for the following 18 weeks to promote hyperlipidaemia and advanced atherosclerosis. Circulating cholesterol levels were measured at baseline (prior to virus administration), 6 and 10-weeks post injection and at sacrifice. Consistent with previous studies validating the AAV-PCSK9-induced model in wild-type animals [3][4], we found increased cholesterol levels in $CARMN^{+/+}$ and $CARMN^{-/-}$ animals compared to baseline, demonstrating efficacy of the model (Online Figure VII E). We found no differences in body weight and plasma cholesterol in $CARMN^{-/-}$ versus $CARMN^{+/+}$ animals (Online Figure VII F, G). Additionally, we did not observe significant differences in circulating immune cells and bone marrow progenitors in the two groups of animals, suggesting little or no effect on immune cell differentiation and proliferation (Online Figure VIII, IX, X). We next evaluated the severity of atherosclerosis by histological analysis in cross-sections in two of the main sites where atherosclerosis develops in mice, the brachiocephalic arteries and the aortic roots. To specifically evaluate the structure and the volume of the lesions in the brachiocephalic arteries, we used Optical Projection Tomography (OPT) [5]. Quantification of the resulting 3-dimensional images showed increased plaque volumes in $CARMN^{-/-}$ animals compared to wild type controls (Figure 6

D). Analysis of Haematoxylin/Eosin stained section confirmed an increase in plaque area in the brachiocephalic arteries of CARMN$^{-/-}$ versus CARMN$^{+/+}$ mice (Figure 6 E-F). Furthermore, we observed a significant increase of the cross-sectional area of the lesions developed in the aortic roots of CARMN$^{-/-}$ versus control mice (Figure 6 G-H). We next sought to characterize the composition of the plaques in the brachiocephalic artery and aortic roots. In the pathological setting, abnormal proliferation of vSMCs [4 3] and resident macrophages [48 49] represent a key features of developing plaques. Cellular proliferation was analysed by EdU incorporation. A significant increase in EdU incorporation was observed in the plaques of CARMN$^{-/-}$ animals compared to controls (Figure 7 A, B) and thus increased proliferation rate of cells within the plaques. To further analyse the cellular composition of the plaques, cross-sections of the brachiocephalic arteries were stained for markers of vSMCs Acta2, Myh11, and a marker for activated macrophages and de-differentiated vSMCs, Lgals3. While the overall amount of smooth muscle actin-expressing vSMCs and cells positive for Myh11 was similar among the CARMN$^{+/+}$ and CARMN$^{-/-}$ groups (Figure 7 C-D and Online Figure X C, D), the content of Lgals3 in the plaque was found to be significantly increased in the lesions of CARMN$^{-/-}$ versus wild type controls (Figure 7 E-F). Moreover, the process of collagen deposition/degradation is a determinant factor in evaluating the structure and the stability of the plaques and can be used as measure of plaque vulnerability [50,51]. Therefore, we investigated the impact of CARMN$^{-/-}$ on the collagen turnover. Picrosirius red staining of the brachiocephalic arteries showed a significant decrease in collagen in CARMN$^{-/-}$ versus CARMN$^{+/+}$ animals, in line with decreased collagen gene expression observed *in vitro*. (Figure 7 G, H). However, no significant change was observed in the plaque composition of the aortic roots of CARMN$^{-/-}$ versus wild type controls (Online Figure VII H-K). The absence of significant differences between the CARMN$^{-/-}$ and CARMN$^{+/+}$ groups at the aortic root level could be explained by the vascular-site specific or temporal differences during plaque formation [52]. Overall, these data suggest that the depletion of *CARMN* induced the progression of atherosclerotic lesions to a more vulnerable plaque type.

DISCUSSION

Here, we comprehensively characterized for the first time the expression and the function of the *CARMN* lncRNA loci in hCASMC phenotypes *in vitro* and identified the functional consequence of the genetic loss of this lncRNA in the pathological setting of atherosclerosis *in vivo*. We show that GapmeR-mediated loss of the lncRNA primes vSMCs into a pro-pathological activated state, with concomitant reduction in the expression levels of both miR-143 and miR-145. Moreover, we functionally dissected the roles of *CARMN* and the miR-143/145 cluster and highlighted that in addition to its role as microRNA host gene, our data suggest that the *CARMN* lncRNA has miRNA-independent effects on vSMCs function. Furthermore, we show loss of *CARMN* in advanced human and mouse atherosclerotic lesions compared to matched tissue with stable and less advanced disease regions. Finally, we show that CRISPR/Cas9-mediated genetic targeting of *CARMN* in mice leads to development of more advanced lesions in cholesterol-fed mice.

We used an RNA sequencing approach to understand the functional consequence of the modulation of *CARMN* lncRNA expression *in vitro* in hCASMCs. Our results reveal that the loss of *CARMN* lncRNA expression significantly affects the transcriptional vSMC landscape. In particular, following *CARMN* knockdown, hCASMCs gained a gene expression signature associated with a partially differentiated state towards a more plastic phenotype, and showed a dysregulation of fundamental biological processes such as proliferation and migration. Transcriptomic analysis of *CARMN* at basal condition showed a substantial overlap with CMBCD-loaded signature, particularly in metabolism and homeostasis of lipids. Accordingly, we postulated that depletion of *CARMN* predisposes hCASMCs to acquire early phenotypic/functional properties of foam-cell like cells, thus priming the pro-atherogenic phenotype likely contributing to the pathophysiology of CVD. However, the dedifferentiation process following *CARMN* and miR-143/145

depletion affected only some of the vSMC identity markers indicating a partial effect towards de-differentiating phenotype.

Recent studies have begun to unravel the complex network of interactions between those miRNAs that are embedded within so-called host genes[26], whose biogenesis can be mutually exclusive [27] or they can be co-expressed and exert independent functions [28]. In our study, we observed the expression of miR-143 and miR-145 was also affected by *CARMN* depletion. This effect could simply be due to the pri-miRNA precursor overlapping *CARMN* locus. On the other hand, it is also possible the existence of a regulatory circuit in which *CARMN* represents an additional level of post-transcriptional regulation and its downregulation affects the expression level of the miRNAs. We acknowledge that the presence of multiple promoters identified for the miRNAs[16,20] enhances the challenge to uncover the existing lncRNA-miRNAs regulatory mechanisms. A recent study highlighted the possibility for lncRNA host genes to regulate hosted miRNAs via super-enhancer regulatory regions[53] and *CARMN* was previously shown to be associated with a super-enhancer region and to increase its activity[24]. However, the demonstration of the cis-regulatory role of *CARMN* in vSMCs would require further studies, including chromatin marks and interaction analysis in this cell type. In addition, the literature on the regulation and function of these miRNAs in atherosclerosis is unclear.

We used a co-transfection strategy to increase the levels of miR-143/145 in *CARMN*-depleted vSMCs, allowing to dissect the contribution of *CARMN* from the miRNAs *in vitro.* Albeit the off-target limitation of the co-transfection strategy, our findings suggest that *CARMN* regulation of vSMC proliferation may possibly occur independently of the modulation of miR-143/145 expression. However, further dissociation of *CARMN* and miR-143 and miR-145 effect remains experimentally challenging due to the genetic complexity of the locus. Hence, further studies are required to understand the independent effects of *CARMN* and mir143/145 using, for example, targeted CRISPR activation, inhibition and editing approaches on the locus in primary vascular cells and mice. Our data expands the knowledge on the expression of the lncRNA at early and advanced stages of human and mouse atherosclerotic plaques. In a clinical setting, *CARMN* was significantly downregulated in advanced plaques versus stable lesions isolated by endarterectomy from symptomatic patients. Additionally, *CARMN* expression was found significantly reduced in murine advanced atheroma versus fatty streak. Therefore, we suggest that the downregulation of *CARMN* is a key event associated with the progression to more advanced lesions in CVD.

To determine whether the functional role of the lncRNA is conserved *in vivo,* and to understand the functional consequence of the loss of *CARMN* during the pathophysiology of atherosclerosis *in vivo*, we genetically modulated the expression of the lncRNA in mice exploiting the CRISPR/Cas9 technology. Previous studies have genetically ablated a region of the pre-miRNAs stem loop to generate miR-143/145-deficent mice [14,15,17,19]. We targeted the promoter region of the locus encompassing the first exon of *CARMN* transcripts. This resulted in the first genetic CARMN$^{-/-}$ model. In our *in vivo* atherosclerosis study using CARMN$^{-/-}$ mice, we found increased cellular proliferation in the atherosclerotic lesions of CARMN$^{-/-}$ versus CARMN$^{+/+}$ animals and a more advanced plaque phenotype in the CARMN$^{-/-}$ mice. This result can be explained by findings from previous studies where vSMCs within advanced plaque show high proliferative index[54,55,56.] The evaluation of plaque composition revealed a largely unchanged content of typical vSMC markers, *α-SMA* and *MYH11*. However, considering that expression of vSMC differentiation markers, such as *α-SMA* and *Myh11*, are lost by dedifferentiated vSMCs in advanced plaques [7], the interpretation of these results is limited as vSMC may no longer be recognised as such. Recent advances in vSMC-fate mapping have allowed a more reliable identification of vSMC-derived cells which contribute to intimal and atherosclerotic lesions formation in injured arteries[57,58]. We acknowledge the lack of lineage-tracing mouse model represents a limitation to unambiguously characterize the plaque composition in our *in vivo* study. The evaluation of *Lgals3*, marker for macrophages and dedifferentiated vSMCs revealed a significant increase in CARMN$^{-/-}$ versus CARMN$^{+/+}$ animals. Recently, studies have provided evidence that the rapid turnover and build-up of macrophages in advanced atherosclerotic plaques is mostly due to their local

proliferation [48,59]. Importantly, the large pool of foamy and pro-inflammatory cells expressing Lgals3, was defined among the main features of lesion progression toward the advanced state [38]. Accordingly, our results show that CARMN$^{-/-}$ increases the content of Lgals3, thus inducing the progression of the plaques toward an inflammatory and advanced stage. Collectively, these results reveal the functional role of *CARMN* axis to the phenotype observed *in vivo* and to clearly define the contribution of *CARMN* and microRNAs separately is an area for future research.

The decrease in collagen content within the lesions has been associated with progression to a more advanced plaque phenotype [60]. In this context, previous studies have reported that lower content of collagen may be due to a reduced synthesis by vSMCs and to an enhanced degradation by metalloproteases and collagenases [50]. In our study, the analysis of total collagen content within the plaques showed a significant decrease in CARMN$^{-/-}$ versus CARMN$^{+/+}$ mice, confirming that CARMN$^{-/-}$ induced a more advanced plaque phenotype. These results are consistent with the transcriptomic analysis of hCASMCs following knock-down of *CARMN*, where we observed a decrease in collagen and elastase gene expression and the upregulation of genes associated with collagen breakdown (MMPs).

Collectively, our study demonstrates that loss of *CARMN* axis is an early event in atherosclerosis, both in mice and human. We have shown that downregulation of *CARMN* is detrimental for the maintenance of hCASMCs differentiated state and induces itself a phenotypic transition toward pro-proliferative phenotype, independently from the modulation of miR-143/145 cluster. In this research, we have characterized the effect of the dysregulation of miR-143/145 on the expression of vSMC identity genes and their ability to migrate. Finally, we have characterized the phenotypical consequence of *CARMN* depletion during the development of atherosclerosis *in vivo* and demonstrated that the knock-out of *CARMN* locus altered the composition of the plaques to a more advanced plaque type.

ACKNOWDLEGEMENTS

The authors thank Gregor Aitchison, Kathryn Newton, Michael Millar, Erwin Wijnands and George Kuriakose for their technical assistance during the study. Flow cytometry data were generated with support from the QMRI Flow Cytometry and cell sorting facility, University of Edinburgh. AAV8-PCSK9 was kindly provided by the AVU (AAV Vector Unit), I.C.G.E.B (Trieste, TS). Laser Capture Microdissection was performed in collaboration with Professor Ira Tabas at Columbia University Medical Centre (NY) and with the technical assistance of the Confocal and Specialized Microscopy Shared Resource, Columbia University Medical Centre (NY). The authors also thank Prof. Martyn Taylor, Stefan Rooke and Amanda Warr for the assistance provided during the Oxford Nanopore sequencing and data analysis.

SOURCES OF FUNDING

This work is supported by the British Heart Foundation Research Excellent Award [RE/18/5/34216], BHF Chair [CH/11/2/28733] and fellowship to F.V. (FS/18/10/33413), and a BHF programme Grant to A.H.B [BHF CVR grant (RM/17/3/33381)] and the European Research Council Advanced Grant VASMIR (RE7644) to A.H.B., and Dutch heart foundation fellowship 2016T060 and a Leducq transatlantic network grant to J.C.S. and BHF project grant to A.H.B and L.D. This project has also received funding from the European Union's Horizon 2020 Programme for Research and Innovation (825670). T.C.W is the recipient of a Wellcome Trust award [204802/Z/16/Z]. Australian National Health and Medical Research Council Early Career Fellowship [APP1072662 to M.B.C]

DISCLOSURES

MBC has received support from Oxford Nanopore Technologies (ONT) to present at scientific conferences. However, ONT played no role in study design, execution, analysis or publication.

SUPPLEMENTAL MATERIALS
Expanded Methods
Online figures I-X
Online Dataset I-VI

REFERENCES

1. Stefanadis C, Antoniou CK, Tsiachris D, Pietri P. Coronary atherosclerotic vulnerable plaque: Current perspectives. *J. Am. Heart Assoc*. 2017;6.
2. Owens GK, Kumar MS, Wamhoff BR. Molecular regulation of vascular smooth muscle cell differentiation in development and disease. *Physiol. Rev*. 2004;84:767–801.
3. Gomez D, Owens GK. Smooth muscle cell phenotypic switching in atherosclerosis. *Cardiovasc. Res*. 2012;95:156–164.
4. Bennett MR, Sinha S, Owens GK. Vascular Smooth Muscle Cells in Atherosclerosis. *Circ Res*. 2016;118:692–702.
5. Wang Y, Dubland JA, Allahverdian S, Asonye E, Sahin B, Jaw JE, Sin DD, Seidman MA, Leeper NJ, Francis GA. Smooth Muscle Cells Contribute the Majority of Foam Cells in ApoE (Apolipoprotein E)-Deficient Mouse Atherosclerosis. *Arterioscler Thromb Vasc Biol*. 2019;39:876–887.
6. Newby AC, Zaltsman AB. Fibrous cap formation or destruction - The critical importance of vascular smooth muscle cell proliferation, migration and matrix formation. *Cardiovasc. Res*. 1999;41:345–360.
7. Allahverdian S, Chaabane C, Boukais K, Francis GA, Bochaton-Piallat ML. Smooth muscle cell fate and plasticity in atherosclerosis. *Cardiovasc. Res*. 2018;114:540–550.
8. Mahmoud AD, Ballantyne MD, Miscianinov V, Pinel K, Hung J, Scanlon JP, Iyinikkel J, Kaczynski J, Tavares AS, Bradshaw AC, Mills NL, Newby DE, Caporali A, Gould GW, George SJ, Ulitsky I, Sluimer JC, Rodor J, Baker AH. The human-specific and smooth muscle cellenriched LncRNA SMILR promotes proliferation by regulating mitotic CENPF mRNA and drives cell-cycle progression which can be targeted to limit vascular remodeling. *Circ Res*. 2019;125:535–551.
9. Cremer S, Michalik KM, Fischer A, Pfisterer L, Jaé N, Winter C, Boon RA, Muhly-Reinholz M, John D, Uchida S, Weber C, Poller W, Günther S, Braun T, Li DY, Maegdefessel L, Perisic Matic L, Hedin U, Soehnlein O, Zeiher A, Dimmeler S. Hematopoietic deficiency of the long noncoding RNA malat1 promotes atherosclerosis and plaque inflammation. *Circulation*. 2019;139:1320–1334.
10. Hung J, Scanlon JP, Mahmoud AD, Rodor J, Ballantyne M, Fontaine MAC, Temmerman L, Kaczynski J, Connor KL, Bhushan R, Biessen EAL, Newby DE, Sluimer JC, Baker AH. Novel plaque enriched long noncoding RNA in atherosclerotic macrophage regulation (PELATON). *Arterioscler Thromb Vasc Biol*. 2020;40:697–713.
11. Vengrenyuk Y, Nishi H, Long X, Ouimet M, Savji N, Martinez FO, Cassella CP, Moore KJ, Ramsey SA, Miano JM, Fisher EA. Cholesterol loading reprograms the microRNA-143/145-Myocardin axis to convert aortic smooth muscle cells to a dysfunctional macrophage-like phenotype. *Arterioscler Thromb Vasc Biol*. 2015;35:535–546.
12. Quintavalle M, Elia L, Condorelli G, Courtneidge SA. MicroRNA control of podosome formation in vascular smooth muscle cells in vivo and in vitro. *J Cell Biol*. 2010;189:13–22.
13. Vacante F, Denby L, Sluimer JC, Baker AH. The function of miR-143, miR-145 and the MiR-143 host gene in cardiovascular development and disease. *Vascul. Pharmacol*. 2019;112:24–30.
14. Boettger T, Beetz N, Kostin S, Schneider J, Krüger M, Hein L, Braun T. Acquisition of the contractile phenotype by murine arterial smooth muscle cells depends on the Mir143/145 gene cluster. *J Clin Invest*. 2009;119:2634–2647.
15. Elia L, Quintavalle M, Zhang J, Contu R, Cossu L, Latronico MVG, Peterson KL, Indolfi C, Catalucci D, Chen J, Courtneidge SA, Condorelli G. The knockout of miR-143 and -145 alters

smooth muscle cell maintenance and vascular homeostasis in mice: Correlates with human disease. *Cell Death Differ*. 2009;16:1590–1598.
16. Cordes KR, Sheehy NT, White MP, Berry EC, Morton SU, Muth AN, Lee TH, Miano JM, Ivey KN, Srivastava D. MiR-145 and miR-143 regulate smooth muscle cell fate and plasticity. *Nature*. 2009;460:705–710.
17. Xin M, Small EM, Sutherland LB, Qi X, McAnally J, Plato CF, Richardson JA, Bassel-Duby R, Olson EN. MicroRNAs miR-143 and miR-145 modulate cytoskeletal dynamics and responsiveness of smooth muscle cells to injury. *Genes Dev*. 2009;23:2166–2178.
18. Lovren F, Pan Y, Quan A, Singh KK, Shukla PC, Gupta N, Steer BM, Ingram AJ, Gupta M, Al-Omran M, Teoh H, Marsden PA, Verma S. MicroRNA-145 targeted therapy reduces atherosclerosis. *Circulation*. 2012;126:S81-90.
19. Cipollone F, Felicioni L, Sarzani R, Ucchino S, Spigonardo F, Mandolini C, Malatesta S, Bucci M, Mammarella C, Santovito D, De Lutiis F, Marchetti A, Mezzetti A, Buttitta F. A unique MicroRNA signature associated with plaque instability in humans. *Stroke*. 2011;42:2556–2563.
20. Deng L, Blanco FJ, Stevens H, Lu R, Caudrillier A, McBride M, McClure JD, Grant J, Thomas M, Frid M, Stenmark K, White K, Seto AG, Morrell NW, Bradshaw AC, MacLean MR, Baker AH. MicroRNA-143 Activation Regulates Smooth Muscle and Endothelial Cell Crosstalk in Pulmonary Arterial Hypertension. *Circ Res*. 2015;117:870–883.
21. Caruso P, Dempsie Y, Stevens HC, McDonald RA, Long L, Lu R, White K, Mair KM, McClure JD, Southwood M, Upton P, Xin M, Van Rooij E, Olson EN, Morrell NW, MacLean MR, Baker AH. A role for miR-145 in pulmonary arterial hypertension: Evidence from mouse models and patient samples. *Circ Res*. 2012;111:290–300.
22. Rangrez AY, Massy ZA, Meuth VM Le, Metzinger L. MiR-143 and miR-145 molecular keys to switch the phenotype of vascular smooth muscle cells. *Circ Cardiovasc Genet*. 2011;4:197–205.
23. Lagarde J, Uszczynska-Ratajczak B, Carbonell S, Pérez-Lluch S, Abad A, Davis C, Gingeras TR, Frankish A, Harrow J, Guigo R, Johnson R. High-throughput annotation of full-length long noncoding RNAs with capture long-read sequencing. *Nat Genet*. 2017;49:1731–1740.
24. Ounzain S, Micheletti R, Arnan C, Plaisance I, Cecchi D, Schroen B, Reverter F, Alexanian M, Gonzales C, Ng SY, Bussotti G, Pezzuto I, Notredame C, Heymans S, Guigó R, Johnson R, Pedrazzini T. CARMEN, a human super enhancer-associated long noncoding RNA controlling cardiac specification, differentiation and homeostasis. *J Mol Cell Cardiol*. 2015;89:98–112.
25. Plaisance I, Perruchoud S, Fernandez-Tenorio M, Gonzales C, Ounzain S, Ruchat P, Nemir M, Niggli E, Pedrazzini T. Cardiomyocyte Lineage Specification in Adult Human Cardiac Precursor Cells Via Modulation of Enhancer-Associated Long Noncoding RNA Expression. *JACC Basic to Transl Sci*. 2016;1:472–493.
26. Profumo V, Forte B, Percio S, Rotundo F, Doldi V, Ferrari E, Fenderico N, Dugo M, Romagnoli D, Benelli M, Valdagni R, Dolfini D, Zaffaroni N, Gandellini P. LEADeR role of miR-205 host gene as long noncoding RNA in prostate basal cell differentiation. *Nat Commun*. 2019;10.
27. Legnini I, Morlando M, Mangiavacchi A, Fatica A, Bozzoni I. A Feedforward Regulatory Loop between HuR and the Long Noncoding RNA linc-MD1 Controls Early Phases of Myogenesis. *Mol Cell*. 2014;53:506–514.
28. Sun Q, Tripathi V, Yoon JH, Singh DK, Hao Q, Min KW, Davila S, Zealy RW, Li XL, Polycarpou-Schwarz M, Lehrmann E, Zhang Y, Becker KG, Freier SM, Zhu Y, Diederichs S, Prasanth SG, Lal A, Gorospe M, Prasanth K V. MIR100 host gene-encoded lncRNAs regulate cell cycle by modulating the interaction between HuR and its target mRNAs. *Nucleic Acids Res*. 2018;46:10405–10416.
29. Ulitsky I, Bartel DP. XLincRNAs: Genomics, evolution, and mechanisms. *Cell*. 2013;154:26.
30. Ponting CP, Oliver PL, Reik W. Evolution and Functions of Long Noncoding RNAs. *Cell*. 2009;136:629–641.
31. Deaton RA, Gan Q, Owens GK. Spl-dependent activation of KLF4 is required for PDGF-BB-induced phenotypic modulation of smooth muscle. *Am J Physiol - Hear Circ Physiol*.

2009;296:H1027-1037.
32. Chellan B, Reardon CA, Getz GS, Bowman MAH. Enzymatically modified low-density lipoprotein promotes foam cell formation in smooth muscle cells via macropinocytosis and enhances receptor-mediated uptake of oxidized low-density lipoprotein. *Arterioscler Thromb Vasc Biol*. 2016;36:1101–1113.
33. Miano JM. Myocardin in biology and disease. *J Biomed Res*. 2015;29:3–19.
34. Ait-Oufella H, Taleb S, Mallat Z, Tedgui A. Recent advances on the role of cytokines in atherosclerosis. *Arterioscler Thromb Vasc Biol*. 2011;31:969–979.
35. van der Vorst EPC, Döring Y, Weber C. Chemokines and their receptors in Atherosclerosis. *J. Mol. Med*. 2015;93:963–971.
36. Adiguzel E, Ahmad PJ, Franco C, Bendeck MP. Collagens in the progression and complications of atherosclerosis. *Vasc. Med*. 2009;14:73–89.
37. Newby AC. Metalloproteinases and Vulnerable Atherosclerotic Plaques. *Trends Cardiovasc. Med*. 2007;17:253–258.
38. Shankman LS, Gomez D, Cherepanova OA, Salmon M, Alencar GF, Haskins RM, Swiatlowska P, Newman AAC, Greene ES, Straub AC, Isakson B, Randolph GJ, Owens GK. KLF4-dependent phenotypic modulation of smooth muscle cells has a key role in atherosclerotic plaque pathogenesis. *Nat Med*. 2015;21:628–637.
39. Duband JL, Gimona M, Scatena M, Sartore S, Small JV. Calponin and SM22 as differentiation markers of smooth muscle: spatiotemporal distribution during avian embryonic development. *Differentiation*. 1993;55:1–11.
40. Zhang H, Jiang M, Liu Q, Han Z, Zhao Y, Ji S. miR-145-5p inhibits the proliferation and migration of bladder cancer cells by targeting TAGLN2. *Oncol Lett*. 2018;16:6355–6360.
41. Zhu H, Dougherty U, Robinson V, Mustafi R, Pekow J, Kupfer S, Li YC, Hart J, Goss K, Fichera A, Joseph L, Bissonnette M. EGFR signals downregulate tumor suppressors miR-143 and miR-145 in western diet-promoted murine colon cancer: Role of G 1 regulators. *Mol Cancer Res*. 2011;9:960–975.
42. Koltsova EK, Hedrick CC, Ley K. Myeloid cells in atherosclerosis: A delicate balance of anti-inflammatory and proinflammatory mechanisms. *Curr. Opin. Lipidol*. 2013;24:371–380.
43. Stary HC, Chandler AB, Glagov S, Guyton JR, Insull W, Rosenfeld ME, Schaffer SA, Schwartz CJ, Wagner WD, Wissler RW. A definition of initial, fatty streak, and intermediate lesions of atherosclerosis: A report from the committee on vascular lesions of the council on arteriosclerosis, American Heart Association. *Arterioscler Thromb*. 1994;14:840–856.
44. Falk E. Pathogenesis of Atherosclerosis. *J. Am. Coll. Cardiol*. 2006;47:C7-12.
45. Maxwell KN, Breslow JL. Adenoviral-mediated expression of Pcsk9 in mice results in a low-density lipoprotein receptor knockout phenotype. *Proc Natl Acad Sci U S A*. 2004;101:7100–7105.
46. Bjørklund MM, Hollensen AK, Hagensen MK, Dagnæs-Hansen F, Christoffersen C, Mikkelsen JG, Bentzon JF. Induction of atherosclerosis in mice and hamsters without germline genetic engineering. *Circ Res*. 2014;114:1684–1689.
47. Kirkby NS, Low L, Seckl JR, Walker BR, Webb DJ, Hadoke PWF. Quantitative 3-dimensional imaging of murine neointimal and atherosclerotic lesions by optical projection tomography. *PLoS One*. 2011;6.
48. Robbins CS, Hilgendorf I, Weber GF, Theurl I, Iwamoto Y, Figueiredo JL, Gorbatov R, Sukhova GK, Gerhardt LMS, Smyth D, Zavitz CCJ, Shikatani EA, Parsons M, Van Rooijen N, Lin HY, Husain M, Libby P, Nahrendorf M, Weissleder R, Swirski FK. Local proliferation dominates lesional macrophage accumulation in atherosclerosis. *Nat Med*. 2013;19:1166–1172.
49. Jenkins SJ, Ruckerl D, Thomas GD, Hewitson JP, Duncan S, Brombacher F, Maizels RM, Hume DA, Allen JE. IL-4 directly signals tissue-resident macrophages to proliferate beyond homeostatic levels controlled by CSF-1. *J Exp Med*. 2013;210:2477–2491.
50. Rekhter MD. Collagen synthesis in atherosclerosis: Too much and not enough. *Cardiovasc. Res*. 1999;41:376–384.

51. Rekhter MD. How to evaluate plaque vulnerability in animal models of atherosclerosis? *Cardiovasc. Res*. 2002;54:36–41.
52. VanderLaan PA, Reardon CA, Getz GS. Site Specificity of Atherosclerosis: Site-Selective Responses to Atherosclerotic Modulators. *Arterioscler. Thromb. Vasc. Biol*. 2004;24:12–22.
53. Suzuki HI, Young RA, Sharp PA. Super-Enhancer-Mediated RNA Processing Revealed by Integrative MicroRNA Network Analysis. *Cell*. 2017;168:1000-1014.e15.
54. Doran AC, Meller N, McNamara CA. Role of smooth muscle cells in the initiation and early progression of atherosclerosis. *Arterioscler. Thromb. Vasc. Biol.* 2008;28:812–819.
55. Chappell J, Harman JL, Narasimhan VM, Yu H, Foote K, Simons BD, Bennett MR, Jørgensen HF. Extensive Proliferation of a Subset of Differentiated, yet Plastic, Medial Vascular Smooth Muscle Cells Contributes to Neointimal Formation in Mouse Injury and Atherosclerosis Models. *Circ Res*. 2016;119:1313–1323.
56. Dobnikar L, Taylor AL, Chappell J, Oldach P, Harman JL, Oerton E, Dzierzak E, Bennett MR, Spivakov M, Jørgensen HF. Disease-relevant transcriptional signatures identified in individual smooth muscle cells from healthy mouse vessels. *Nat Commun*. 2018;9.
57. Majesky MW, Horita H, Ostriker A, Lu S, Regan JN, Bagchi A, Dong XR, Poczobutt J, Nemenoff RA, Weiser-Evans MCM. Differentiated Smooth Muscle Cells Generate a Subpopulation of Resident Vascular Progenitor Cells in the Adventitia Regulated by Klf4. *Circ Res*. 2017;120:296–311.
58. Feil S, Fehrenbacher B, Lukowski R, Essmann F, Schulze-Osthoff K, Schaller M, Feil R. Transdifferentiation of vascular smooth muscle cells to macrophage-like cells during atherogenesis. *Circ Res*. 2014;115:662–667.
59. Lutgens E, De Muinck ED, Kitslaar PJEHM, Tordoir JHM, Wellens HJJ, Daemen MJAP. Biphasic pattern of cell turnover characterizes the progression from fatty streaks to ruptured human atherosclerotic plaques. *Cardiovasc Res*. 1999;41:473–479.
60. Barnes MJ, Farndale RW. Collagens and atherosclerosis. *Exp Gerontol*. 1999;34:513–525.

FIGURE LEGENDS

Figure 1. *CARMN* expression in basal and stimulated human primary CASMCs.
A) Schematic representation of human *CARMN* splice variants and pre-miRNAs miR-143 and miR-145 based on ENSEMBL version (GRCh38/hg38), including the position of the forward (Fw) and reverse (Rev) primers used to amplify all transcripts, grey arrows (except 4, 10 and 11) and the target region for the GapmeRs, GapCARMN, GapCARMN2 and GapCARMN3. The black arrows next to each transcript name, indicate the direction of transcription. B) Expression levels of *CARMN* transcripts in hCASMCs (n=3) via qRT-PCR using isoform-specific primers (Isoform 1,2,3,4+9,5,6,7,8,9,10,11, and 12) and common primers (amplifying all isoforms except 4, 10 and 11). C) Diagram of hCASMCs in basal condition (0.2% FBS) and treated for 48 hours with PDGF-BB. Histogram plots obtained by FACS showing the percentage of hCASMCs (n=3) up-tacking EdU following PDGF-BB treatment and in basal (0.2% FBS) conditions. Student's t-test was used to assess statistical significance indicated with p values. D) QRT-PCR to show expression of *CARMN*, miR-143 and miR-145 in hCASMCs (n=3) treated with PDGF-BB. Student's t-test was used to assess statistical significance indicated with p values. E) Diagram of the wound healing assay performed in hCASMCs (n=3), representative micrographs of hCASMCs scratch assay and migrating cells (Scale bar 100μm) and qRT-PCR showing the expression of *CARMN* and miR-143/145 G) Diagram of hCASMCs (n=3) in basal condition (0.2% BSA) and treated with cholesterol-methyl-b-cyclodextrin treated for 72 hours and expression levels of dedifferentiation markers (Acta2, Myh11, CD68 and Lgals3), *CARMN* and miR-143/145 by RT-qPCR. Student's t-test was used to assess statistical significance indicated with p values. H) qRT-PCR data showing the expression of *CARMN* and miR-143/145 in basal (0.2% FBS) and following CMBCD-loading treatment. Student's t-test was used to assess statistical significance indicated with p values.

Figure 2. *CARMN*-regulated genes relevant to vSMC proliferation, migration and water-soluble cholesterol dependent dedifferentiation
A) QRT-PCR results showing the expression of *CARMN*, miR-143 and miR145 hCASMCs (n=3) following transfection with GapmeR targeting *CARMN* (GapCARMN) and GapmeR control (GapCTR). Mock indicates un-transfected cells. One-way ANOVA with Bonferroni multiple comparison test was used to assess statistical significance indicated with p values.
B) Schematic representation of the RNA-seq study design. C) Heatmap (as z-score of log2(FPKM+1)) of differentially regulated genes by *CARMN* depletion in all conditions. The purple box highlights the clustering of all *CARMN*_KD samples while the red box shows the CMBCD treated replicates (Cont_KD). D) Graph of selected Go Term (Biological Process). The analysis was performed on the 2315 genes regulated by *CARMN* depletion in any conditions. E) Heatmap (as z-score of log2(FPKM+1)) of selected differentially regulated genes by GapCARMN and GapCTR in the basal condition with the shortest time of GapmeR transfection (migration). F) Venn diagram showing the overlap between genes regulated by *CARMN* depletion (in Basal-C condition) and genes regulated by CMBCD treatment (in GapCTR condition) in the same direction.

Figure 3. The knockdown of *CARMN* regulated hCASMC proliferation, migration and dedifferentiation.
A) Representative FACS plots showing the of EdU uptake in hCASMCs transfected with GapmeR targeting *CARMN* (GapCARMN) or GapmeR control (GapCTR). The gate (P4) indicates the EdU positive cells, the samples are named GapmeR negative control (GapCTR) and GapmeR targeting *CARMN* (GapCARMN). B) Percentage of EdU positive hCASMCs (n=3) following transfection with GapCARMN, GapCTR and un-transfected cells (Mock) upon PDGF-BB stimuli and in 0.2% FBS. One-way ANOVA with Bonferroni multiple comparison test was used to assess statistical significance indicated with p values. C) Representative pictures of hCASMCs at 0 and 10 hours from the scratch following transfection with GapCARMN, GapCTR and Mock in 0.2% FBS medium. Pictures were acquired at 10X magnification. Scale bar 100μm. D) Quantification of the relative migration distances of hCASMCs (n=3), obtained using

ImageJ tool. One-way ANOVA with Bonferroni multiple comparison test was used to assess statistical significance indicated with p values.
E), F), G), H) Expression levels of dedifferentiation markers Acta2, Myh11, CD68 and Lgals3 in hCASMCs (n=3) stimulated with water-soluble cholesterol-methyl-b-cyclodextrin (CMBCD) or 0.2% BSA for 72 hours following transfection with GapCARMN, GapCTR or Mock. One-way ANOVA with Bonferroni multiple comparison test was used to assess statistical significance indicated with p values.

Figure 4. *CARMN* depletion regulated hCASMCs phenotypes in miRNAs-dependent and independent mode.
A), B) QRT-PCR expression data of miR-143, miR-145 and *CARMN* relative to housekeeper gene (RNU and UBC respectively) in GapCARMN, control (GapCTR), a combination of GapCARMN and mimic control (Gap+mimicCTR) and a combination of GapCARMN and mimic overexpressing miR143 and miR145 (GapCARMN+mimic143/145). Mock refers to un-transfected control cells. One-way ANOVA with Bonferroni multiple comparison test was used to assess statistical significance indicated with p values. C) Percentage of EdU positive hCASMCs (n=3) evaluated by FACS analysis and analyzed using FlowJo software. One-way ANOVA with Bonferroni multiple comparison test was used to assess statistical significance indicated with p values. D), E), F), G) qRT-PCR expression data relative to Acta2, Myh11, CD68 and Lgals3, respectively relative to housekeeper gene UBC in the above-mentioned transfection conditions. One-way ANOVA with Bonferroni multiple comparison test was used to assess statistical significance indicated with p values. H), I) Quantification of the relative migration distances of hCASMCs (n=3), obtained using ImageJ tool and representative images of hCASMCs at 0 and 10 hours from the induction of the scratch. Images acquired at 10X magnification, scale bar 100μm. One-way ANOVA with Bonferroni multiple comparison test was used to assess statistical significance indicated with p values. ns= not significant.

Figure 5. The *CARMN* locus is downregulated in human and murine atherosclerosis.
A) Expression level of *CARMN* and B) Expression level of MMP1, ELN, IL1-beta, CCL2 as FPKM in paired, stable (n=4) and unstable (n=4) human plaque segments retrieved after endarterectomy from 4 symptomatic patients. P value obtained based on the raw read counts using DESeq2. C) Expression of *CARMN* and miR143/145 in human stable and unstable plaques isolated through endarterectomy (n=4) determined by qRT-PCR. Mann-Whitney was used to assess statistical significance indicated with p values. D) Representative bright field images of in-situ detection of *CARMN* co-localizing with α-SMA, CD68 or CD45 signal in plaques obtained from carotid artery derived from symptomatic patients at carotid endarterectomy. Pictures were acquired consecutively at 4X, 10X and 40X magnification Scale bar 50μm. E) Representative Haematoxylin & Eosin staining of aortic roots isolated from $LDLR^{-/-}$ mice. Pictures were acquired with 4x and 10X magnification. Scale bar 100μm. F) Expression levels of *CARMN* and miR143/145 in fatty streak (n=4) and advanced murine plaques (n=11) isolated by Laser Capture Microdissection. Mann-Whitney was used to assess statistical significance indicated with p values.

Figure 6. Genetic ablation of *CARMN* affects the area, the volume and the composition of plaques developed in the aortic arches of $CARMN^{-/-}$ versus $CARMN^{+/+}$ animals.
Schematic representation of *CARMN* locus located on mouse chromosome 18 and the CRISPR/Cas9 deletion of the first exon and 4.8 kilobases of the promoter (total 5 kilobases). The arrows next to each transcript name, indicate the direction of transcription. The grey arrows and box indicate where common primers to both isoforms were designed. B) Validation of knockout strategy by qRT-PCR using common primer set performed on the aortic arches of $CARMN^{+/+}$ (n=4) and $CARMN^{-/-}$ (n=6) mice. Mann-Whitney was used to assess statistical significance indicated with p values. C) Schematic workflow used for the induction of mouse atherosclerosis using AAV8-mediated overexpression of PCSK9 and high cholesterol diet in $CARMN^{+/+}$ and $CARMN^{-/-}$ animals. D) Representative tomographic reconstruction of pictures obtained by Optical Projection Tomography (black picture) and non-tomographic projection of the mouse aortic arch (white picture). The arrows indicate the brachiocephalic artery. Quantification of the plaque

volumes in $CARMN^{+/+}$ (n=7) and $CARMN^{-/-}$ (n=8) animals performed using CTan software. Student's t-test was used to assess statistical significance indicated with p values. E) Representative Haematoxylin & Eosin staining of cross-sections from brachiocephalic artery of $CARMN^{+/+}$ and $CARMN^{-/-}$ animals. Pictures acquired at 10X magnification. Scale bar 200µm. F) Quantification of the plaque areas at the site of maximum lesion of brachiocephalic arteries in $CARMN^{+/+}$ (n=10) and $CARMN^{-/-}$ (n=9) mice, performed using Fiji software. Student's t-test was used to assess statistical significance indicated with p values. G) Haematoxylin & Eosin staining of cross-sections from aortic roots of wild type and $CARMN^{-/-}$ animals. Pictures acquired at 5X magnification. Scale bar 200µm. H) Quantification of plaque area of aortic roots of $CARMN^{+/+}$ (n=14) and $CARMN^{-/-}$ (n=15) animals, performed using QuPath software. Student's t-test was used to assess statistical significance indicated with p values.

Figure 7. The genetic knock-out of *CARMN* increased the expression of Lgals3 in plaques developed in the aortic arch of $CARMN^{-/-}$ animals versus wild type controls. A) Representative EdU staining of proliferating cells in plaques from $CARMN^{+/+}$ and $CARMN^{-/-}$ animals. Pictures were acquired with 10X magnification. Scale bar 80µm. B) Quantification of proliferating cells in plaques of $CARMN^{+/+}$ (n=10) and $CARMN^{-/-}$ (n=9) animals. Values are expressed as % of positive nuclei over the total cells counted in the plaque. C) and E) Representative immunostainings and D) and F) quantification of the positive area for αSMA and Lgals3 staining respectively in the plaques of $CARMN^{+/+}$ (n=10) and $CARMN^{-/-}$ (n=9) animals. Pictures acquired at 10X magnification. Scale bar 200µm. G) Representative picrosirius red staining and H) quantification of collagen content in the plaques of $CARMN^{+/+}$ (n=10) and $CARMN^{-/-}$ (n=9) animals. The pictures were acquired by polarized light microscopy at 10X magnification. Scale bar 200µm. Student's t-test was used to assess statistical significance indicated with p values.

NOVELTY AND SIGNIFICANCE

What Is Known?

- De-differentiation of vascular smooth muscle cells (vSMCs) occurs in atherosclerotic lesions.
- Non-coding RNAs, such as long non-coding RNAs (lncRNAs) and microRNAs (miRNAs), can regulate key aspects of vascular pathology.
- *CARMN* is a lncRNA located immediately upstream of miRNAs, miR-143 and miR-145, which are involved in vSMC function.

What New Information Does This Article Contribute?

- The CARMN/mir143/mir145 axis can prime vSMCs towards pro-proliferative, pro-migratory and de-differentiated phenotypes, *in vitro.*
- CARMN lncRNA potentially acts independently of the miRNAs to regulate vSMC proliferation, whereas migration and de-differentiation phenotypes are likely modulated by mir143/145 independently.
- CARMN knockout mice develop accelerated atherosclerosis and advanced plaques.

In this study, the conserved and genetically complex long non-coding RNA CARMN, and its co-located miRNAs, miR-143 and miR-145, were comprehensively characterized in human and mouse atherosclerosis. CARMN transcript down-regulation was associated with advanced plaque phenotype and CARMN knockout in mouse had increased atherosclerosis. Downregulation of the CARMN/miR-143/miR-145 axis primed vSMCs towards pro-proliferative, pro-migratory and dedifferentiated phenotypes, *in vitro*. Mechanistically, we provided evidence that the CARMN lncRNA acted independently of the miRNAs to regulate vSMC proliferation, whereas migration and dedifferentiation phenotypes were associated with the modulation of miRNAs expression. While both miRNAs are well known in vSMC biology, our study begins to dissect the complex genetic interplay between lncRNA host genes and their associated miRNAs in health and disease. Further, we provide evidence for the fundamental, yet complex role of lncRNAs in vSMC function.

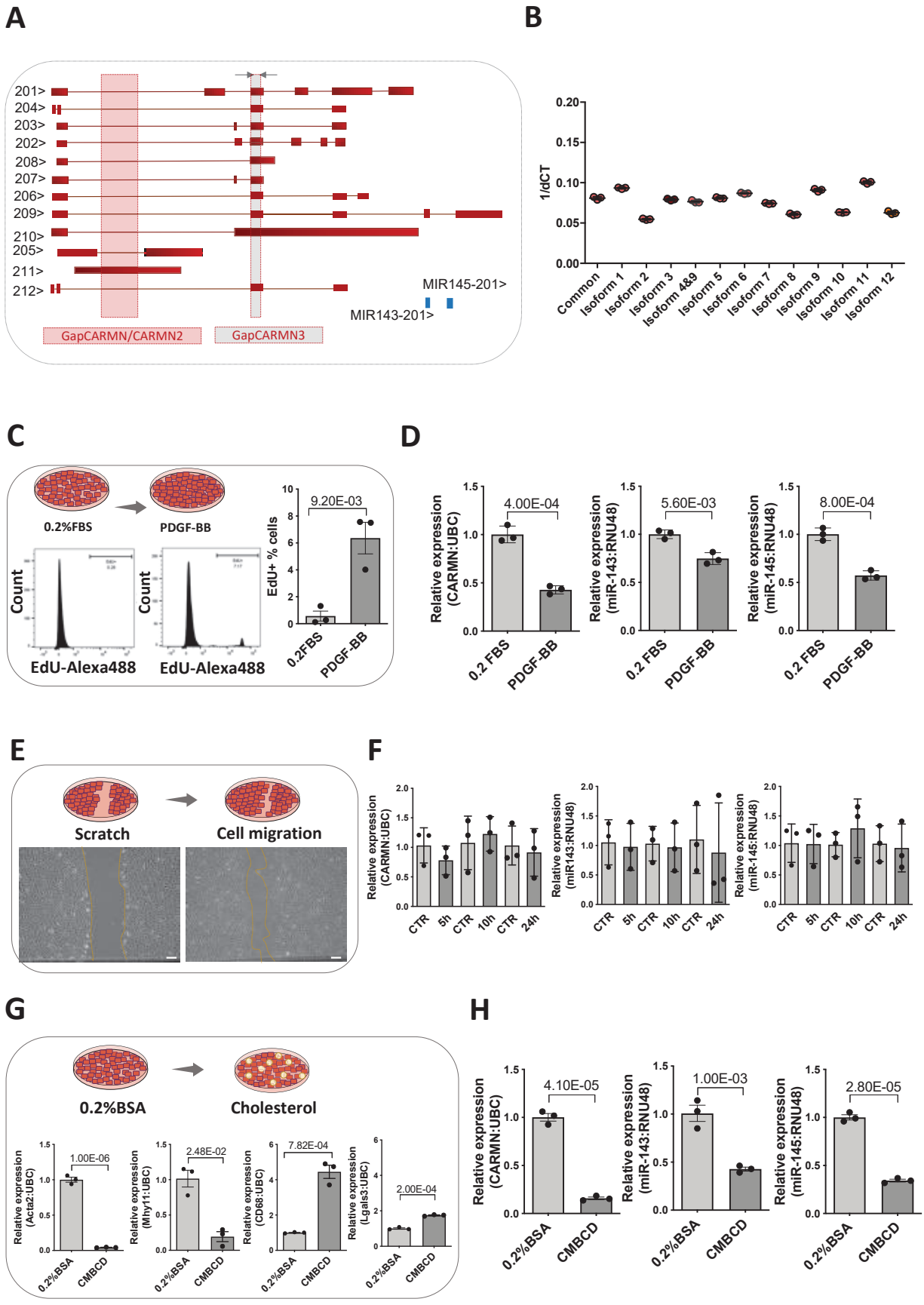

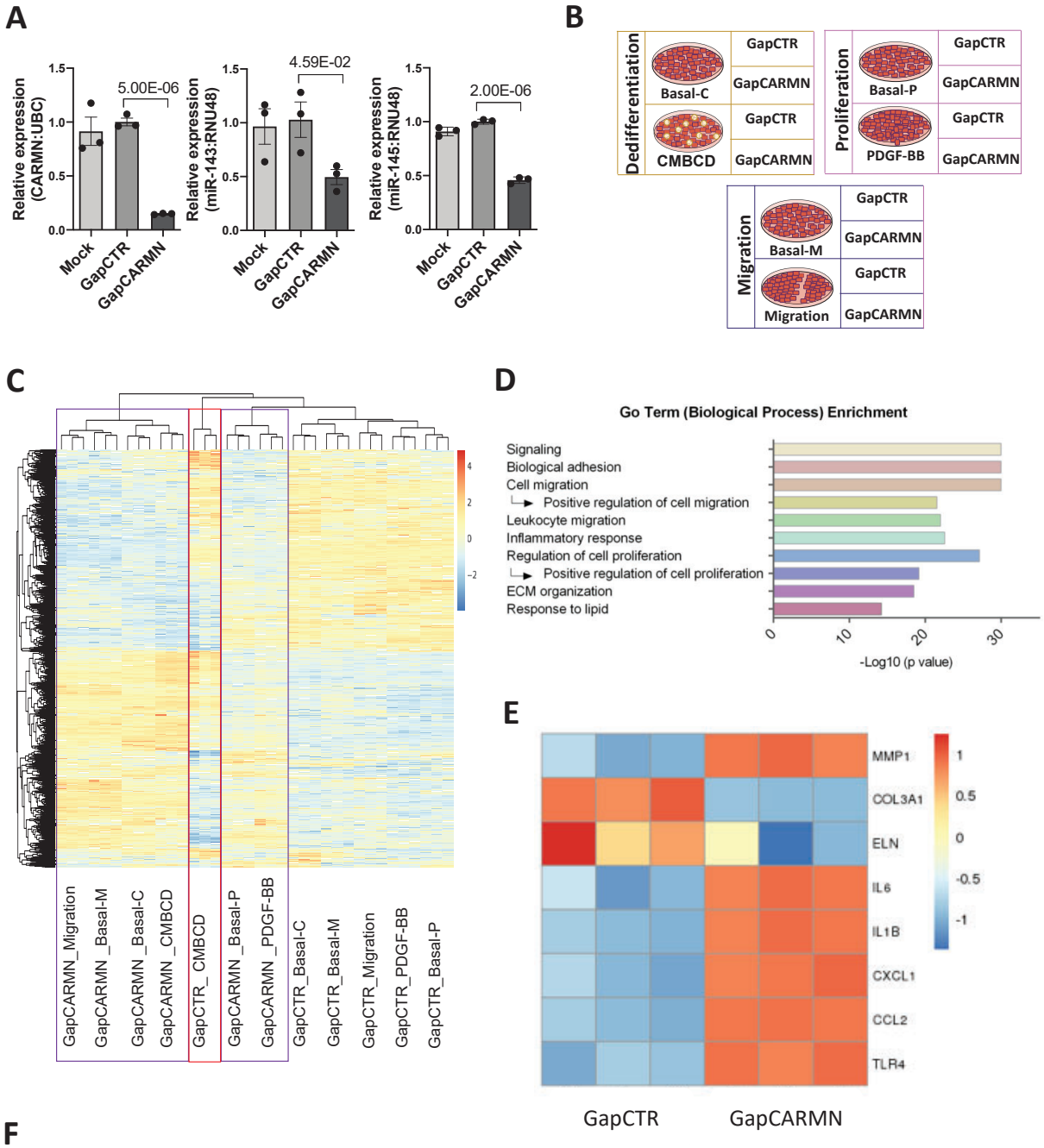

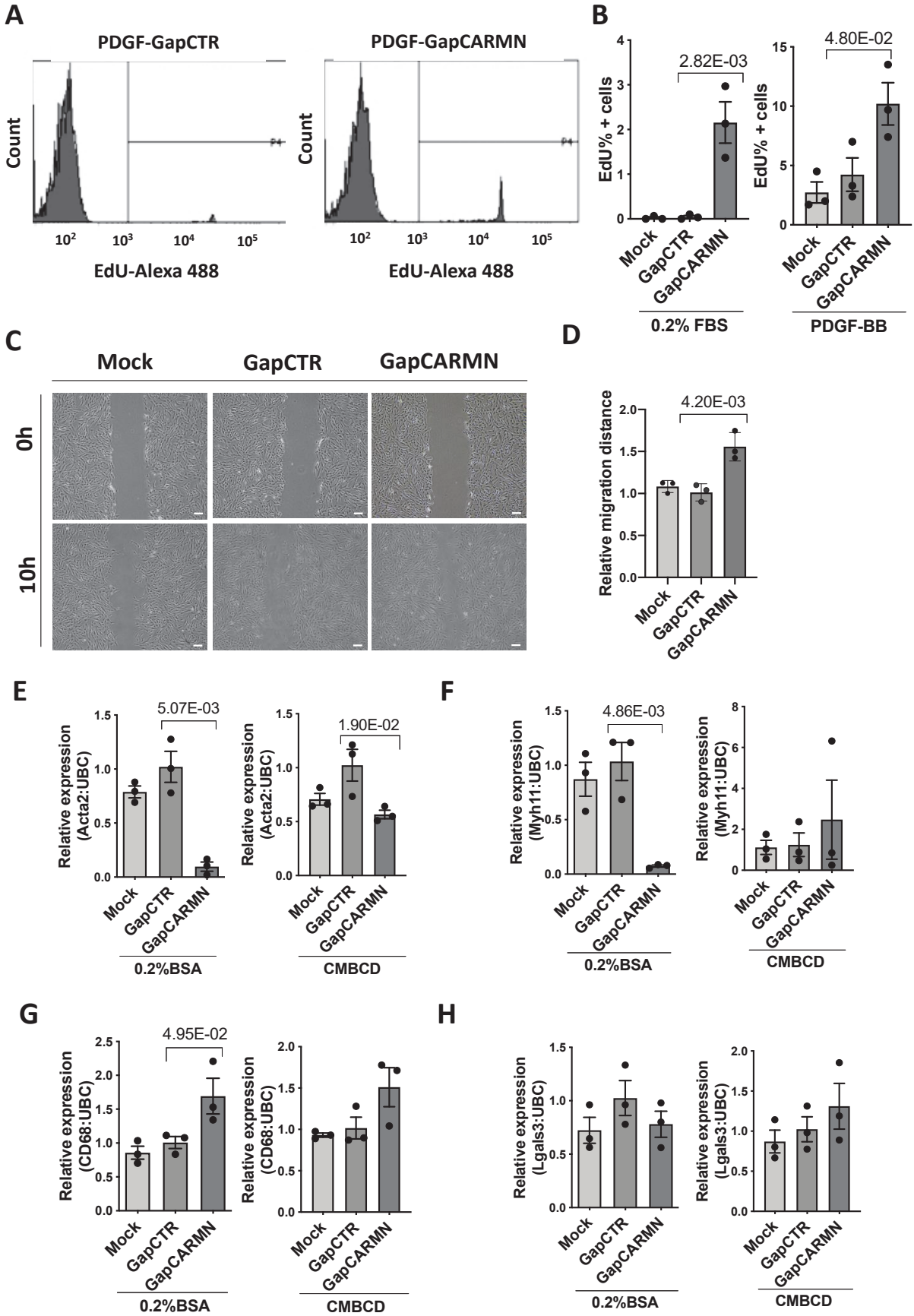

FIGURE 4